# Tuning the Mechanical Properties of Metallopolymers via Ligand Interactions: A Combined Experimental and Theoretical Study

Yuval Vidavsky,<sup>†,||</sup> Michael R. Buche,<sup>†,||</sup> Zachary M. Sparrow,<sup>‡</sup> Xinyue Zhang,<sup>§</sup> Steven J. Yang,<sup>†</sup> Robert A. DiStasio, Jr.,<sup>‡,\*</sup> and Meredith N. Silberstein<sup>†,\*</sup>

†Sibley School of Mechanical and Aerospace Engineering, †Department of Chemistry and Chemical Biology, Baker Laboratory, and §Department of Materials Science and Engineering, Cornell University, Ithaca, New York 14853, United States.

KEYWORDS: Metallopolymers, density functional theory (DFT), mechanical properties, external forces explicitly included (EFEI), polymer design.

ABSTRACT: Metal-ligand interactions provide a means for modulating the mechanical properties of metallopolymers as well as an avenue towards understanding the connection between crosslink interaction strength and macroscale mechanical properties. In this work, we used nickel carboxylate as the tunable crosslinking interaction in a metallopolymer. Different numbers and types of neutral ligands that coordinate to the metal center are introduced as an easy approach to adjust the strength of the ionic interactions in the nickel carboxylate crosslinks, thus allowing macroscale mechanical properties to be tuned. Density functional theory (DFT) calculations, with the external forces explicitly included (EFEI) approach, were used to quantify how the number and type of ligands affect the stiffness, strength, and thermodynamic stability of the nickel carboxylate crosslinking interactions. Interpreting the bulk material properties in the context of these DFT results suggests that the stiffness and strength of the crosslinking interactions primarily control the initial stiffness and yield strength of the metallopolymer, while the mechanical behavior at higher strain is controlled by dynamical bond reformation and interactions with the polymer environment. The physicochemical insight gained from this work can be used in the rational design of metallopolymers with a wide scope of targeted mechanical properties.

### INTRODUCTION

The consolidation of metal cations into a polymer architecture has been demonstrated as an efficient method to modify the mechanical behavior of polymeric materials.<sup>1-4</sup> Organometallic complexes can function as network crosslinkers,<sup>2.5</sup> as part of a linear backbone,<sup>6-8</sup> as grafting points,<sup>9</sup> as the driving force for phase segregation,<sup>10,11</sup> and even as intrachain crosslinkers in organic nanoparticles.<sup>11,12</sup> The metal-ligand interactions that form these complexes can vary from weak, dynamic bonds to strong, covalent-like bonds that are effectively static.<sup>7</sup> This range of bond strengths makes the use of these complexes a flexible and robust approach for controlling the mechanical properties of polymers.<sup>14</sup> Further, these complexes can impart desirable characteristics such as self-healing<sup>15-17</sup> and stimuli responsiveness<sup>18-20</sup> that are not usually achievable with covalent bonding alone. Several studies have shown that the stability and mechanical strength of these interactions in metallopolymers can be tuned by using either different metal cations or different binding ligands.<sup>1,2,6,21</sup> However, tuning the mechanical properties of polymers with these methods often requires new synthetic routes and processing methods. As such, a facile method is needed for modulating the metal-ligand interaction, and hence the mechanical properties of polymers.

In addition, an understanding of how the nature of metal-ligand interactions influence macroscale mechanical behavior will allow for more effective materials design to suit specific applications. Metal complexes fall within a broader class of force sensitive bonded interactions.<sup>8,13,16,21-28</sup> Extensive computational and theoretical work has been conducted over the last 20 years to quantify the stiffness, strength, and force-dependent kinetics of mechanochemically sensitive bonds.<sup>29-35</sup> In this regard, density functional theory (DFT) based computational approaches such as COGEF (constrained geometry to simulate forces),<sup>29,36</sup> AISMD (*ab initio* steered molecular dynamics),<sup>37</sup> and EFEI<sup>31</sup> (external forces explicitly included) have been invaluable in the design of materials that incorporate these bonds.<sup>38-40</sup>

In this work, we present a simple technique for easily adjusting the strength of ionic crosslinking interactions between Ni<sup>2+</sup> cations and the carboxylate anions on the backbone of an acrylic polymer. In particular, we study how the attachment of neutral ligands to the crosslinking metal center weaken the ionic interaction and alter the macroscale mechanical properties. By combining DFT calculations with bulk experiments, we provide a fundamental understanding of how changes in the number and type of ligands can be used to tune the mechanical properties of the bulk polymer. Theoretical analysis enables us to identify which features of the bulk mechanical behavior can be tuned by modifying the strength and stiffness of the crosslinks, and which features can be tuned from changing the ligand-environment interactions. These findings have broad implications for the design of polymers with dynamic crosslinks and the possibility for secondary interactions to dominate aspects of the mechanical response. In doing so, we provide a facile and rational design procedure that uses ligands to create a versatile class of metallopolymers with highly tunable bulk mechanical properties.

### RESULTS AND DISCUSSION

Nickel Carboxylate Crosslinked Network Synthesis and Characterization. All polymers were synthesized by 365 nm UV-initiated free radical copolymerization of the acrylic formulation in a dog-bone shape silicone mold pressed between two laminated glass plates (Figures S1 and S2). For the Ni<sup>2+</sup> crosslinked network (Ni), the acrylic formulation was prepared by dissolving nickel(II) acetate tetrahydrate salt (Ni(OAc)<sub>2</sub>(H<sub>2</sub>O)<sub>4</sub>) in a mixture of 2-hydroxyethyl acrylate (HEA) and 2-carboxyethyl acrylate (CEA); see Supporting Information. HEA serves as a hydrophilic neutral monomer and the CEA reacts with the Ni<sup>2+</sup> cations to generate the ionic crosslinker after removal of the acetic acid under vacuum (Scheme 1). The quantity of Ni(OAc)<sub>2</sub>(H<sub>2</sub>O)<sub>4</sub> was chosen to provide a 1:2 ratio of Ni<sup>2+</sup>:CEA. The combination of a fast curing process, a hydrophilic monomer composition that is compatible with the nickel cations, and a synthesized polymer with a glass transition temperature ( $T_g$ ) above ambient temperature ensure homogeneous dispersion of the Ni<sup>2+</sup> throughout the polymer bulk and suppress potential phase segregation.<sup>41</sup> The linear copolymer (Linear) was synthesized under the same conditions without the addition of the nickel salt. In addition, homopolymers of HEA with and without Ni(OAc)<sub>2</sub>(H<sub>2</sub>O)<sub>4</sub> were synthesized as controls (Ni\* and Linear\* in Scheme 1), since they cannot generate nickel carboxylate crosslinkers.

**Scheme 1.** (Top) Copolymer synthesis with (**Ni**) and without (**Linear**) nickel crosslinking. (Bottom) Control/Homopolymer synthesis with (**Ni\***) and without (**Linear\***) dispersed nickel.

The successful attachment of nickel cations to the carboxylate crosslinkers was determined by the peak shift of the C=O bond stretching vibration in the IR spectrum. The **Linear** and **Linear\*** polymers show only one peak at ~1724 cm<sup>-1</sup> for the C=O stretching vibration of the backbone ester groups and the free carboxylic acid (Figure 1a). For the **Ni** and **Ni\*** polymers, an additional peak is present at ~1581 cm<sup>-1</sup>, corresponding to the nickel carboxylate bonds<sup>42</sup> in these systems.

Nickel crosslinking in the copolymer results in an increase in the  $T_g$  from 33.9 °C to 42.5 °C, as measured by dynamic mechanical analysis (DMA) (Figure S3). In contrast to this relatively small  $T_g$  change, nickel crosslinking has a dramatic effect on the mechanical properties of the copolymer. Figure 1b shows the stress-strain curve of the Ni and Linear copolymers (as well as the Ni\* and Linear\* homopolymers) under uniaxial tensile stress at a strain rate of 0.114/s. Here, we find that the non-cross-linked Linear copolymer presents typical behavior for a lightly crosslinked or entangled elastomer. By introducing nickel crosslinking, we find that Ni is characterized by a 15-fold increase in stiffness (4.11 to 62.6 MPa) and yield stress (0.213 to 3.03 MPa), as well as a substantial reduction in elongation (from 596% to 156%) when compared to the Linear copolymer. This Ni behavior is reminiscent of a thermoplastic elastomer. Furthermore, the Ni\* control homopolymer has only a slightly stiffer response than Linear\*, thereby corroborating our hypothesis that nickel carboxylate crosslinking is responsible for the dramatic changes in the mechanical properties.

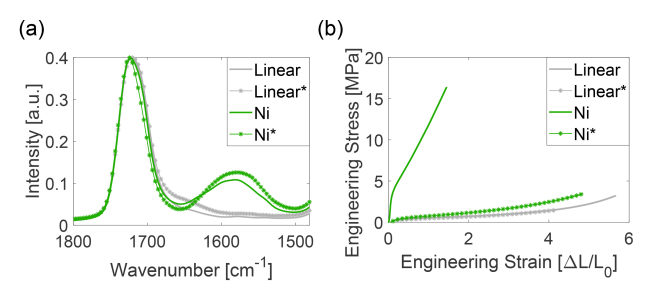


Figure 1. Effects of nickel crosslinking on (a) the IR spectrum and (b) the uniaxial tensile monotonic stress-strain response.

Effects of Ligand Addition. We next sought to modulate the bulk mechanical properties of Ni by altering the stiffness and strength of the nickel carboxylate crosslinks. Our hypothesis here was that the introduction of ligands that are higher in the spectrochemical series than water – which originally stabilizes the octahedral coordination structure of the nickel – would bind more strongly to the metal centers, and thereby displace some of the bound water molecules into the second coordination sphere. Doing so would increase the electron density on the metal centers, and therefore weaken the ionic nickel carboxylate crosslinking interactions. As such, we chose imidazole (Im) as the first ligand to investigate because it is higher in the spectrochemical series<sup>43</sup> than water and is known to coordinate with Ni<sup>2+</sup> cations.<sup>1,5,44</sup>

To further investigate how the introduction of imidazole ligands weakens the nickel carboxylate bonds, we utilized density functional theory (DFT) calculations (in conjunction with the external forces explicitly included (EFEI) procedure<sup>31</sup>) to study the structures and energetics associated with stretching the nickel carboxylate crosslinks in the presence of an external force. All EFEI calculations were performed on a series of model systems with molecular formula Ni(OAc)<sub>2</sub>(H<sub>2</sub>O)<sub>4-n</sub>(Im)<sub>n</sub>, with decoordinated water ligands kept in the second coordination sphere (for n > 0). The lowest energy configurations for all of these model systems involved a triplet wavefunction and an octahedral geometry surrounding the Ni center, with monodentate ( $\kappa^1$ ) and axial binding of the two OAc ligands. Throughout this work, we will refer to these model systems as **Model[Ni]** (for n = 0) and **Model[Im<sub>n</sub>]** (for n = 1, 2, 3, 4). Following geometry optimizations of the initial **Model[Ni]** and **Model[Im<sub>n</sub>]** structures

in the absence of any external forces (see Figure 2a), equal and opposite tensile forces (F) of increasing magnitude were applied to the methyl carbon atoms on the acetate (OAc) moieties, which were taken to represent the attachment points to the polymer (see Figure 2b). In the presence of these external forces (which were incrementally increased by  $\Delta F = 0.1$  nN), these structures were reoptimized for each increment in accordance with the EFEI procedure<sup>31</sup> to obtain the length change in the nickel carboxylate crosslinking site (taken as the distance between the methyl carbon atoms on the OAc groups). These applied forces were increased until one of the nickel carboxylate bonds ruptured (see Figure 2b). All DFT calculations were carried out in Qchem<sup>45</sup> (v5.1) using the dispersion-inclusive range-separated hybrid  $\omega$ B97X-V<sup>46</sup> functional and the def2-TZVPP<sup>47</sup> basis set (see Supporting Information for additional computational details).

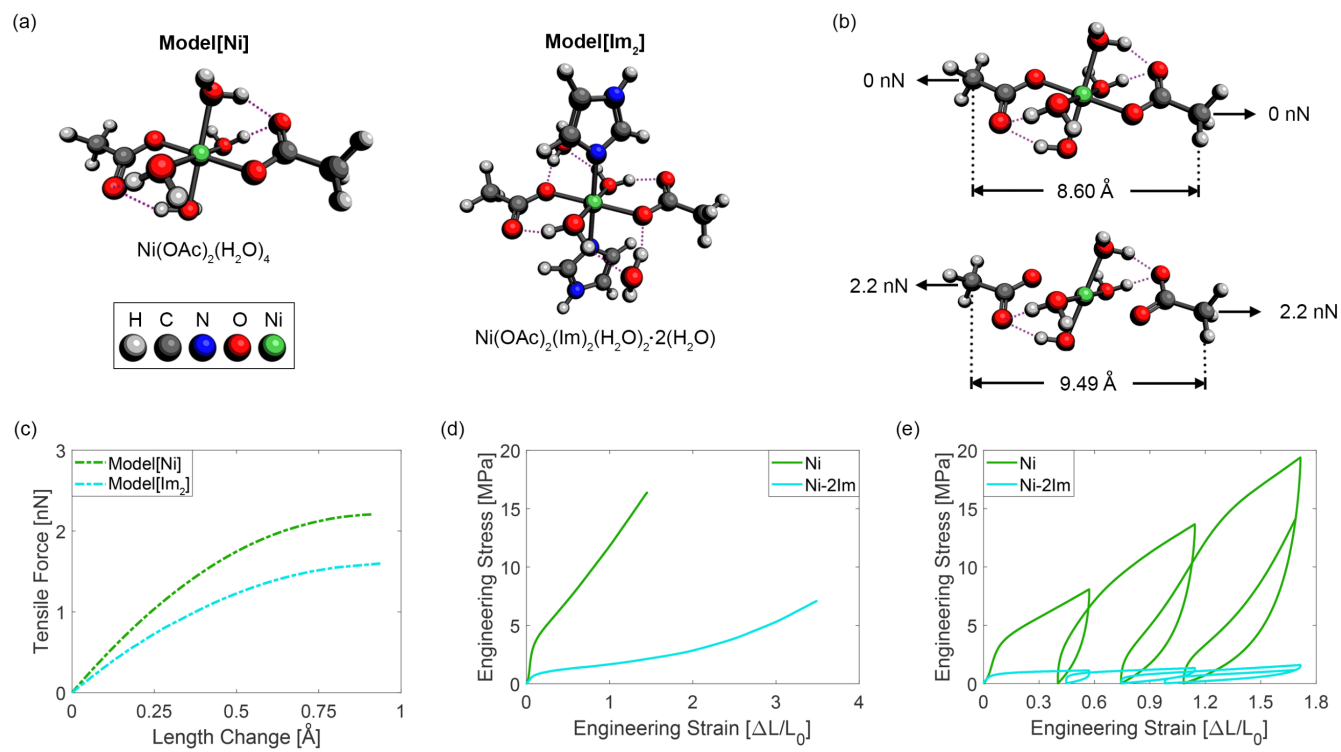


Figure 2. Effects of adding neutral imidazole ligands. (a) Theoretically optimized model systems for the nickel carboxylate crosslinking structure in the absence (Model[Ni]) and presence (Model[Im2]) of two imidazole ligands (with dotted purple lines indicating hydrogen bonds). (b) Starting with the optimized structure, equal and opposite tensile forces were applied to the OAc groups in these model systems until one of the nickel-carboxylate bonds ruptures. (c) Theoretical mechanical responses of the Model[Ni] and Model[Im2] systems using the EFEI approach. (d) Experimental monotonic stress-strain response in the absence (Ni) and presence (Ni-2Im) of two equivalents of imidazole. (e) Experimental cyclic stress-strain response of the Ni and Ni-2Im materials.

As depicted in the theoretically determined mechanical response curves in Figure 2c, we find that Model[Ni] has a linear initial response with a stiffness of 4.5 nN/Å (taken as the initial slope), and a rupture force of 2.2 nN. With two imidazole ligands strongly bound to the metal center, the initial stiffness and rupture force of  $Model[Im_2]$  decrease to 3.1 nN/Å and 1.6 nN, respectively. In order to consider the possible effect that this change in the crosslink stiffness will induce in the bulk

polymer, we performed a molecular dynamics (MD) simulation to estimate the mechanical response of the backbone segment between crosslinks (i.e., which is comprised of seven repeat units of HEA monomers on average). This polymer segment was found to have an initial stiffness of 0.4 nN/Å and a maximum tangent stiffness of 2.4 nN/Å (see Figure S4). Given that the crosslink stiffness is within an order of magnitude of the backbone stiffness, the crosslink will not act as an effectively rigid connection until rupture; hence, we expect that changes in the crosslink stiffness will influence the bulk polymer stiffness. The reduction in the crosslink strength should reduce the bulk polymer yield strength and increase ductility since this crosslink rupture force is below that of a carbon-carbon bond along the backbone.

These model systems were also used to quantify the thermodynamics and kinetics associated with rupturing the nickel carboxylate crosslinks. In particular, we computed the free energy differences ( $\Delta G$ ) and barriers ( $\Delta G^{\ddagger}$ ) between the intact and ruptured configurations of the **Model[Ni]** and **Model[Im2]** systems in the absence of external forces (see Table 1). To obtain the ruptured configuration for each model system, we performed an additional geometry optimization of the structure produced during the final step of the EFEI procedure (in which one of the nickel carboxylate bonds ruptures). With force-free  $\Delta G$  values of +5.06 kcal/mol (**Model[Ni]**) and +6.29 kcal/mol (**Model[Im2]**), our calculations indicate that intact configurations of the nickel carboxylate crosslinks are preferred over ruptured configurations at equilibrium (*i.e.*, crosslink rupturing processes are not spontaneous). Furthermore, we also found that the force-free barriers ( $\Delta G^{\ddagger}$ ) to rupturing these model crosslinks were 18.13 kcal/mol and 15.60 kcal/mol for **Model[Ni]** and **Model[Im2]**, respectively. This observed reduction in  $\Delta G^{\ddagger}$  in **Model[Im2]** is consistent with our hypothesis that the introduction of free imidazole ligands will weaken the effective nickel carboxylate bond strength. We also note that these  $\Delta G^{\ddagger}$  values are large enough such that crosslink rupturing processes will not occur at room temperature due to thermal fluctuations alone.

**Table 1.** Theoretically computed free energy differences ( $\Delta G$ ) and barriers ( $\Delta G^{\ddagger}$ ) between the intact and ruptured configurations of the model systems.

System	ΔG (kcal/mol)	ΔG <sup>‡</sup> (kcal/mol)
Model[Ni]	5.06	18.13
Model[Im <sub>2</sub> ]	6.29	15.60
Model[MeIm <sub>2</sub> ]	4.68	15.36
Model[Py2]	5.21	16.63
Model[Pipe <sub>2</sub> ]	5.95	16.33
Model[DMA <sub>2</sub> ]	6.51	16.66

Inspired by these findings, we performed a series of mechanical tests on the nickel carboxylate crosslinked polymer (Ni) in the presence of two equivalents of neutral imidazole ligands per cation (Ni-2Im). Following the expected trends from the DFT calculations, we observed decreases in the initial modulus (62.56 MPa to 8.36 MPa) and yield stress (3.03 MPa to 0.692 MPa) in going from Ni to Ni-2Im (Figure 2d). Since load is transmitted through the polymer in an indirect manner, it is expected that these bulk property changes are not directly proportional to the crosslink-scale changes in initial stiffness and rupture strength; however, it is a bit surprising that an  $\sim$ 30% decrease in crosslink stiffness leads to an  $\sim$ 87% decrease in the bulk polymer modulus. This suggests that there is a mechanical coupling between the crosslink and the polymer backbone, wherein the backbone becomes effectively more compliant as the crosslink becomes less rigid. This coupling was also suggested by the slight decrease in  $T_g$  observed upon addition of free imidazole ligands. We interpret the yield stress as primarily resulting from the sudden rupture of a large percentage of the crosslinks, and the post-yield hardening as largely resulting from the formation of new crosslinks. Following this interpretation, Ni-2Im requires less stress to break the crosslinks and more time to reform them as compared to Ni. Under cyclic loading (Figure 2e), both materials exhibit extensive viscoplastic deformation. There is also a substantial loss in the overall strength of Ni-2Im, which is visible in the reduced stress of the cyclic stress-strain response as compared to that of monotonic loading (Figure S5). This likely results from an overall loss in intact crosslinks and perhaps associated chain relaxation. The **Ni** cyclic stress response shows a dramatic reduction in yield strength upon each reload, but then dramatically hardens to approach its monotonic response as strain is increases past the prior loading level. This difference in behavior of the Ni-2Im and Ni indicates that the crosslinks reform more slowly when imidazole ligands are bound to the metal center.

Effects of Varying the Number of Ligands. We next sought to obtain further control over these mechanical properties by tuning the number of ligands that were bound to the metal center. We again chose imidazole as the ligand and synthesized three additional polymers with one (Ni-1Im), three (Ni-3Im), and four (Ni-4Im) equivalents of imidazole ligands per nickel. The existence of nickel carboxylate crosslinking interactions in all of the polymers with added imidazole ligands was confirmed by the presence of a C=O stretching vibrational peak at slightly smaller frequency compared to Ni<sup>42</sup> (~1560 cm<sup>-1</sup> in the IR spectra, Figure S8). In addition, changes in the color of the Ni<sup>2+</sup> containing materials (Figure S9) further corroborate the presence of interactions between the imidazole ligands and the metal center. In order to study the effects of varying the number of imidazole ligands on the stiffness and strength of the nickel carboxylate crosslinks, we first needed to investigate how many imidazole ligands were attached to the metal centers in the Ni-1Im, Ni-2Im, Ni-3Im, and Ni-4Im cases.

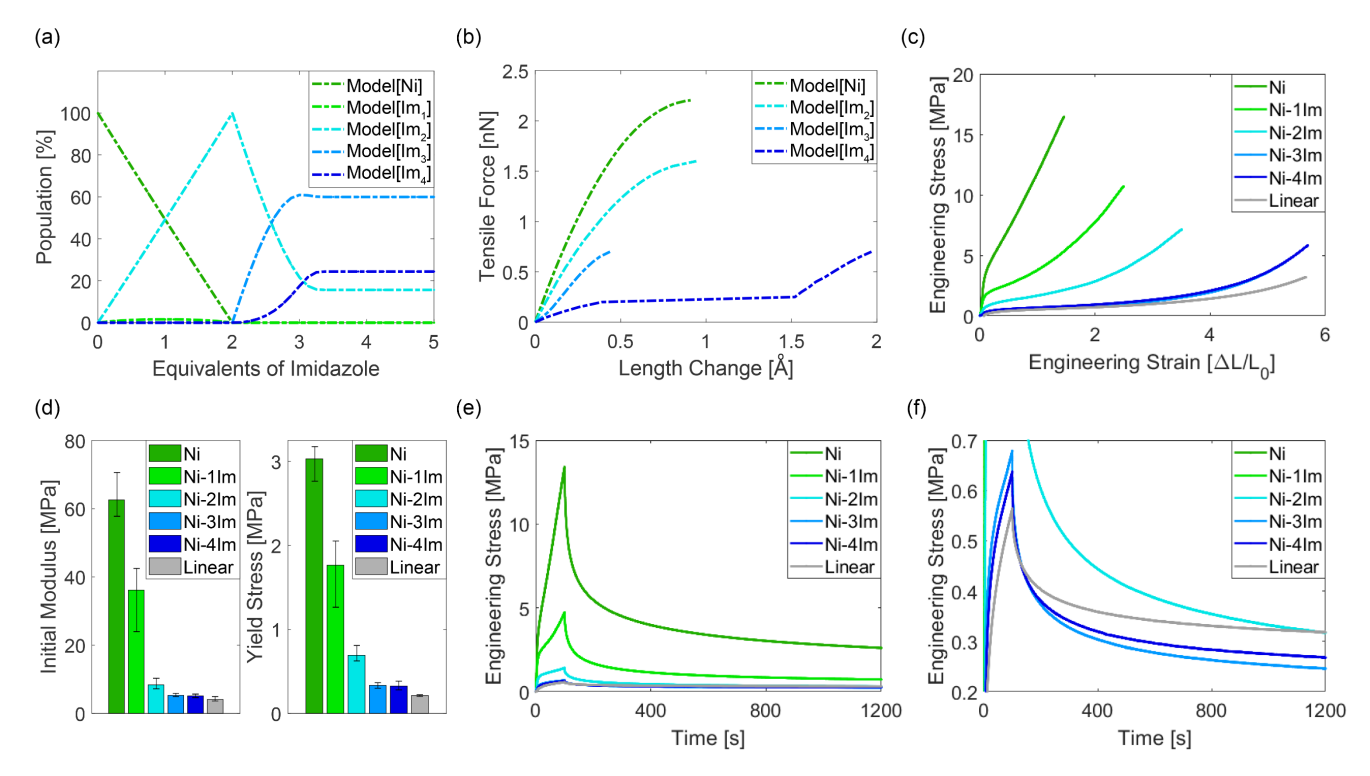


**Figure 3.** Effects of varying the number of imidazole ligands. (a) Theoretically computed equilibrium population of the **Model[Ni]** and **Model[Im<sub>n</sub>]** (for n = 1, 2, 3, 4) systems as a function of the added number of imidazole equivalents. (b) Theoretical mechanical responses of the **Model[Ni]** and **Model[Im<sub>n</sub>]** systems using the EFEI approach. (c) Experimental monotonic stress-strain response of the **Ni**, **Ni-nIm**, and **Linear** materials. (d) Initial modulus and yield stress of these materials. (e) Experimental stress relaxation response of **Ni-2Im**, **Ni-3Im**, **Ni-4Im** and **Linear** (zoomed in compared to subfigure (e)).

To proceed, we used DFT to compute binding free energies ( $\Delta G_{bind}[n]$ ) for the *consecutive* addition of n imidazole ligands to the **Model[Ni]** system (Figure S6, see Supporting Information for additional details). Quite interestingly, this theoretical analysis showed that binding the first and second imidazole ligands was quite favorable, with  $\Delta G_{bind}[1]$  and  $\Delta G_{bind}[2]$  values of -4.60 kcal/mol and -8.34 kcal/mol, respectively. As indicated by  $\Delta G_{bind}[2] > \Delta G_{bind}[1]$ , binding a second imidazole is cooperative in nature. With  $\Delta G_{bind}[3]$  and  $\Delta G_{bind}[4]$  values of -0.80 kcal/mol and +0.53 kcal/mol, we find that it is significantly less favorable to bind a third or fourth imidazole. We attribute these findings to a combination of electronic and steric effects, as the progressive binding of imidazole ligands increases the electron density on the metal and leads to a more crowded complex. With these  $\Delta G_{bind}$  values in hand, we computed the equilibrium populations of **Model[Ini]** and **Model[Imi]** (for n = 1, 2, 3, 4) as a function of the added number of imidazole equivalents (see Supporting Information for additional details). As depicted in Figure 3a, we find that the equilibrium population of **Model[Ini]** rapidly decreases as imidazole is added to the system. This is accompanied by a rapid increase in the population of **Model[Imi]**, while the population of **Model[Imi]** remains at a small and constant (essentially steady-state) value, which is consistent with cooperative binding of the second ligand. Following the addition of three equivalents, we find that the populations of **Model[Im2]**, **Model[Im3]**, and **Model[Im4]** converge to  $\sim 16\%$ ,  $\sim 60\%$ , and  $\sim 24\%$ , respectively, which is consistent with the slightly endergonic binding of the fourth imidazole.

As depicted in the theoretically determined mechanical response curves in Figure 3b (obtained using the EFEI procedure), we find that the initial stiffness and rupture force decrease from 3.1 nN/Å and 1.6 nN (Model[Im<sub>2</sub>]) to 1.2 nN/Å and 0.7 nN (Model[Im<sub>3</sub>]) and 0.74 nN/Å and 0.7 nN (Model[Im<sub>4</sub>]). We note in passing that the EFEI curve for Model[Im<sub>1</sub>] was not computed, since the population of this species was negligible (Figure 3a). Interestingly, the EFEI curve for Model[Im<sub>4</sub>] is relatively flat over a large length change (0.5-1.5 Å); we attribute this to a sudden extension of the carboxylate moieties, which were folded inward due to non-bonded interactions. At this point, the response transitions to a more direct pulling on the nickel-carboxylate bonds, wherein Model[Im<sub>4</sub>] is now characterized by a stiffness of ~1.2 nN/Å, and ultimately ruptures at 0.7 nN (which are the same values as Model[Im<sub>3</sub>]). All these observations are consistent with our hypothesis that binding imidazole ligands increases the electron density on the metal and thereby weakens the ionic nickel carboxylate crosslinks.

Consistent with our earlier findings regarding the free energies ( $\Delta G$ ) and barriers ( $\Delta G^{\ddagger}$ ) between the intact and ruptured configurations of **Model[Im3]** and **Model[Im4]** (with force-free  $\Delta G$  values of +2.12 kcal/mol and +2.11 kcal/mol, respectively) are also preferred over ruptured configurations at room temperature. With a force-free  $\Delta G^{\ddagger}$  = 11.57 kcal/mol for **Model[Im3]**, we also find that the barrier to crosslink rupturing remains inaccessible at room temperature. We note in passing that the corresponding  $\Delta G^{\ddagger}$  for **Model[Im4]** was not computed, as the force-free rupture also involves a multi-step mechanism in which the carboxylate groups unfold.

With these theoretical findings in mind, we then performed an additional series of mechanical tests on the Ni-1Im, Ni-3Im, and Ni-4Im polymers. As depicted in Figure 3c, we find that simply varying the number of imidazole ligands allowed us to tune the monotonic stress-strain behavior between the Ni and Linear polymers. This tuning was accomplished without significantly altering the  $T_g$  of the materials (Figure S7). Here, we find that the initial modulus and yield stress both decrease as the number of imidazole equivalents increases from zero (Ni) to three (Ni-3Im) (Figure 3d). With the addition of four imidazole equivalents (Ni-4Im), these quantities level off, but remain slightly above that of the Linear polymer. These findings are consistent with the theoretical population and EFEI analyses (Figure 3a-3b), in that (i) the addition of imidazole ligands weakens the mechanical response of the crosslink structure, and (ii) after the addition of three equivalents, these effects are still present but begin to level off (i.e., once the equilibrium populations converge). Experimental stress relaxation results (Figure 3e-3f) show that although Ni-3Im and Ni-4Im have a similar peak stress to Linear, their relaxation is more substantial as their curves cross over and continue to diverge from the Linear polymer. Although Ni-2Im starts from a much higher stress, this polymer also crosses over Linear during the 20-minute experimental time frame. These results support the notion that the nickel carboxylate crosslinks are dynamic in nature, helping to facilitate stress relaxation by breaking and reforming. Effects of Varying the Types of Ligands. As an alternative approach to tune the mechanical properties of these polymers, we now investigate the effects of varying the types of ligands attached to the metal center. Here we consider four new nitrogen-

based ligands: methylimidazole (MeIm), pyridine (Py), piperidine (Pipe), dimethylamine (DMA). These ligands were chosen to span options in terms of nitrogen atom hybridization ( $sp^2$  and  $sp^3$ ), bulkiness, and potential for  $\pi$ ····X interactions (with X = -H, cation, anion, or  $\pi$ ) and hydrogen bonding with the surrounding polymer environment. In each case, two equivalents of a given ligand were added to form the **Ni-2MeIm**, **Ni-2Py**, **Ni-2Pipe**, and **Ni-2DMA** polymers, and the nickel carboxylate interactions were again verified by the position of the carboxylate C=O vibrational peak in the IR spectra (Figure S10). Binding energy calculations (see Supporting Information for additional details) again confirm that the addition of two equivalents of each ligand to the bulk material corresponds to an equilibrium population that is almost entirely comprised of two ligands bound to each nickel center (Table S1).

DFT calculations were again employed to quantify the mechanics and thermodynamics of the model crosslink structures depicted in Figure 4. The EFEI results predict that adding any two of these nitrogen-based ligands will decrease the initial stiffness and rupture force with respect to **Model[Ni]** (Figure 5a). The theoretical results also predict that the mechanical properties of the crosslink for this set of ligands are very similar, with the largest observed differences being  $\sim$ 0.25 nN/Å (initial stiffness) and  $\sim$ 0.1 nN (rupture force). With  $\Delta G$  and  $\Delta G^{\ddagger}$  values ranging from +4.68 to +6.51 kcal/mol and 15.36 to 16.66 kcal/mol, we again find that intact configurations of these model systems are preferred over ruptured configurations at room temperature, and the barriers to crosslink rupturing always remain thermally inaccessible (Table 1). The experimentally obtained monotonic stress-strain responses are presented in Figure 5b. In the small-strain regime, the addition of any two ligand equivalents results in a dramatic decrease in both the initial modulus and yield stress when compared to **Ni**. However, the differences observed in these properties are rather small among the different ligand types (Figure 5c), which is again consistent with the theoretical EFEI predictions on the model crosslinks. In the large strain regime, however, the monotonic stress-strain responses tend to be quite distinct. Since everything except the added ligands was held constant during the preparation and testing of these materials, and the EFEI calculations only considered single/isolated model crosslinks (and predicted little to no mechanical differences), we hypothesize that these large-strain differences are primarily governed by ligand-environment interactions rather than the mechanical response of the crosslinks.

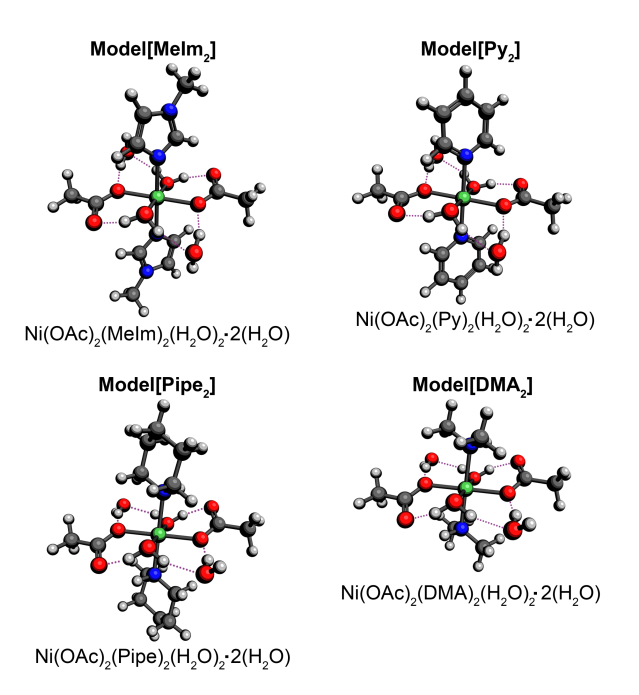
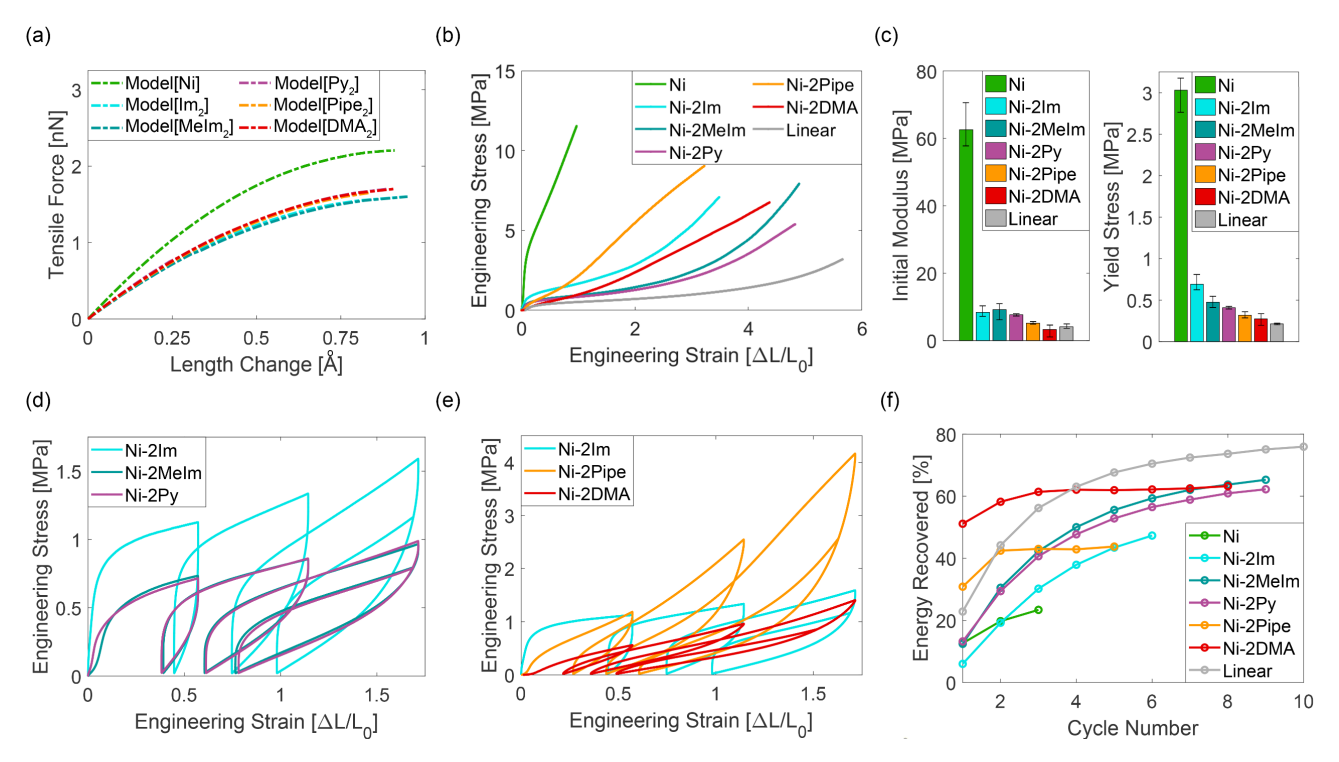


Figure 4. Theoretically optimized model systems for the nickel carboxylate crosslinking structure in the presence of two methylimidazole ( $Model[MeIm_2]$ ), pyridine ( $Model[Py_2]$ ), piperidine ( $Model[Pipe_2]$ ), and dimethylamine ( $Model[DMA_2]$ ) ligands (with dotted purple lines indicating hydrogen bonds).

In fact, one can categorize the stress-strain curves in Figure 5b into the following two groups: (i) Group I polymers (Ni-2Im, Ni-2MeIm, Ni-2Py), which exhibit lower post-yield hardening and smaller instantaneous moduli (until a rapid increase near fracture), and (ii) Group II polymers (Ni-2Pipe, Ni-2DMA), which exhibit higher post-yield hardening and retain near-constant instantaneous moduli until fracture. In this categorization, it is clear that the Group I polymers contain aromatic ligands with  $sp^2$  hybridized (metal-bound) nitrogen atoms, while the Group II polymers contain non-aromatic ligands with  $sp^3$  hybridized nitrogens. Moreover, differences in color among the materials made from these ligands (Figure S11) show a clear categorization into two distinct groups in accordance with the  $sp^2$  vs.  $sp^3$  hybridization of the metal-bound nitrogen atom on each ligand. Since the theoretical EFEI predictions (Figure 5a) show negligible differences in the crosslink mechanical response between ligand types, the hybridization of the (metal-bound) nitrogen does not seem to be directly responsible for the observed differences in the bulk mechanical behavior. However, we can correlate the observed experimental differences in Figure 5b to the distinct non-bonded interactions that can occur between the ligands in each group and the surrounding polymer environment. In other words, the Group I polymers contain aromatic ligands which are capable of forming favorable dispersion (or van der Waals) interactions,  $\pi$ ···X interactions (with X = -H, cation, anion, or  $\pi$ ), and hydrogen bonds (in the case of **Ni-2Im** only) with the environment, while the non-aromatic ligands in the Group II polymers can only form dispersion interactions with the polymer environment. Unlike dispersion interactions (which are radial and non-directional), the  $\pi$ ···X and hydrogen bond interactions present in the Group I polymers are directional and can constrain the diffusion of broken crosslinks throughout the polymer environment. As a result, the rate of dynamic crosslink reformation in the Group I polymers could be substantially lower than that in the Group II polymers. This conjecture is consistent with the monotonic stress-strain curves in Figure 5b, in which the Group I polymers (following the rupture of many crosslinks at yield) are characterized by a lower post-yield hardening (due to the relatively slower crosslink reformation). In contrast, the more rapid crosslink reformation in the Group II polymers manifests as higher post-yield hardening and larger instantaneous moduli until fracture.



**Figure 5.** Effects of varying the types of ligands. (a) Theoretical mechanical responses of the **Model[Ni]**, **Model[Im2]**, **Model[Py2]**, **Model[Pipe2]**, and **Model[DMA2]** systems using the EFEI approach. (b) Experimental monotonic stress-strain response of the **Ni**, **Ni-2Im**, **Ni-2MeIm**, **Ni-2Py**, **Ni-2Pipe**, **Ni-2DMA**, and **Linear** materials. (c) Initial modulus and yield stress of these materials. (d,e) Experimental cyclic stress-strain response of these materials. (f) Percentage of recovered energy per cycle in the cyclic stress-strain experiments.

This explanation for the large-strain monotonic features is also consistent with the observed bulk mechanical responses to cyclic loading. Here, we find that the Group I polymers recover much less than the Group II polymers (Figure 5d,e), as the residual strain (i.e., at zero stress) after each cycle is much smaller for Group II than Group I. We further investigated this point by computing the percentage of recovered mechanical energy per cycle based on the cyclic stress-strain responses (Figure 5f). From these results, we find that the Group II polymers are characterized by a nearly constant energy recovery, which is consistent with breaking and reforming a similar number of crosslinks during each cycle. On the other hand, we find that the Group I polymers are characterized by an initially low recovery percentage that increases rapidly and begins to level off after ~5 cycles. This is also consistent with a slower rate of crosslink reformation among the Group I polymers, in which the energy recovered during each cycle continues to change until most crosslinks are broken. These Group I polymers essentially

transition from a viscoplastic response to an elastomeric one as the crosslinks break, with polymer chains that are effectively linear dominating the response.

Ligand-environment interactions can also be used to rationalize the observed differences within each polymer group. For instance, the mechanical response of Ni-2Im is noticeably different from Ni-2MeIm and Ni-2Py. More specifically, Ni-2Im has a higher yield stress than Ni-2MeIm and Ni-2Py, and maintains this higher stress throughout the strain hardening regime. In this case, the imidazole ligand in Ni-2Im can form hydrogen bonds with the environment (via the non-metal-bound nitrogen atom),<sup>48</sup> while the methylimidazole and pyridine ligands in Ni-2MeIm and Ni-2Py cannot. Furthermore, the similarities between the Ni-2MeIm and Ni-2Py polymers are especially apparent in the cyclic responses, as their curves overlap to within experimental error. Considering the Group II polymers, we find that Ni-2Pipe has a greater strain hardening slope than Ni-2DMA. We attribute this greater mechanical strength of Ni-2Pipe to the increased dispersion interactions between the larger (and significantly more polarizable) piperidine ligand and the surrounding polymer environment.

# **CONCLUSIONS**

In this work, we have demonstrated a facile procedure to incorporate metal-ligand crosslinking in UV-curable acrylic polymers. By attaching a series of coordinating neutral ligands to the metal center, we were able to finely tune the mechanical properties of the polymer. The simplicity of this approach has enabled a systematic investigation of the effects of changing the number and type of coordinating ligands on the crosslink without otherwise modifying the polymer. DFT calculations were used to first determine the number of ligands that would attach as a function of the total ligands available per metal center, and then to investigate the mechanical and thermodynamic characteristics of the equilibrated metal coordination structures. These calculations predicted that the strength and stiffness of the crosslink strongly depend on the number of nitrogen-based ligands, but not on the type. Experimentally, these predictions were borne out in the bulk mechanical behavior at small strain. However, in the strain hardening regime, large differences were observed among the materials with different ligands, suggesting that ligand-environment interactions must also be considered in the rational design process of these versatile and highly tunable polymers.

# ASSOCIATED CONTENT

# **Supporting Information.**

The Supporting Information is available free of charge on the ACS Publications website at DOI:

Synthetic procedures, chemical and mechanical characterization data, material processing, and computational details.

### AUTHOR INFORMATION

# **Corresponding Author**

\*meredith.silberstein@cornell.edu

\*distasio@cornell.edu

### **Author Contributions**

"Y.V. and M.R.B. contributed equally to this work

### **Funding Sources**

This research was funded in part by the National Science Foundation under Grant no. CMMI-1653059 and in part by the Office of Naval Research under Grant no. N00014-17-1-2989 under the administration of PO Dr. Armistead. ZS and RD acknowledge start-up funding from Cornell University. This research made use of the Cornell Center for Materials Research Shared Facilities, which are supported through the NSF MRSEC program (DMR1719875). Calculations in this work used the Extreme Science and Engineering Discovery Environment (XSEDE), which is supported by National Science Foundation grant number ACI-1548562. Calculations were also performed at the Department of Defense (DoD) Supercomputing Resources Centers (DSRCs) through the High Performance Computing Modernization Program (HPCMP).

### Notes

The authors declare no competing financial interest

### **ACKNOWLEDGMENTS**

The authors would like to thank Prathamesh Raiter for his help in running the MD simulations needed to compute the backbone stiffness. The authors would also like to thank Kyle M. Lancaster and Peter T. Wolczanski for helpful scientific discussions.

# REFERENCES

- (1) Grindy, S. C.; Learsch, R.; Mozhdehi, D.; Cheng, J.; Barrett, D. G.; Guan, Z.; Messersmith, P. B.; Holten-Andersen, N. Control of Hierarchical Polymer Mechanics with Bioinspired Metal-Coordination Dynamics. *Nat. Mater.* **2015**, *14* (*12*), 1210–1216.
- (2) Mozhdehi, D.; Neal, J. A.; Grindy, S. C.; Cordeau, Y.; Ayala, S.; Holten-Andersen, N.; Guan, Z. Tuning Dynamic Mechanical Response in Metallopolymer Networks through Simultaneous Control of Structural and Temporal Properties of the Networks. *Macromolecules* **2016**, *49* (17), 6310–6321.
- (3) Filippidi, E.; Cristiani, T. R.; Eisenbach, C. D.; Waite, J. H.; Israelachvili, J. N.; Ahn, B. K.; Valentine, M. T. Toughening Elastomers Using Mussel-Inspired Iron-Catechol Complexes. *Science* **2017**, *358* (6362), 502 505.
- (4) Vidavsky, Y.; Bae, S.; Silberstein, M. N. Modulating Metallopolymer Mechanical Properties by Controlling Metal Ligand Crosslinking. *J. Polym. Sci. Part A Polym. Chem.* **2018**, *56*, 1117–1122.
- (5) Schauser, N. S.; Sanoja, G. E.; Bartels, J. M.; Jain, S. K.; Hu, J. G.; Han, S.; Walker, L. M.; Helgeson, M. E.; Seshadri, R.; Segalman, R. A. Decoupling Bulk Mechanics and Mono- and Multivalent Ion Transport in Polymers Based on Metal-Ligand Coordination. *Chem. Mater.* **2018**, *30* (16), 5759–5769.
- (6) Sha, Y.; Zhang, Y.; Xu, E.; McAlister, C. W.; Zhu, T.; Craig, S. L.; Tang, C. Generalizing Metallocene Mechanochemistry to Ruthenocene Mechanophores. *Chem. Sci.* **2019**, *10* (19), 4959–4965.

- (7) Musgrave, R. A.; Russell, A. D.; Hayward, D. W.; Whittell, G. R.; Lawrence, P. G.; Gates, P. J.; Green, J. C.; Manners, I. Main-Chain Metallopolymers at the Static-Dynamic Boundary Based on Nickelocene. *Nat. Chem.* **2017**, *9* (8), 743–750.
- (8) Sha, Y.; Zhang, Y.; Xu, E.; Wang, Z.; Zhu, T.; Craig, S. L.; Tang, C. Quantitative and Mechanistic Mechanochemistry in Ferrocene Dissociation. *ACS Macro Lett.* **2018**, *7* (10), 1174–1179.
- (9) Rüttiger, C.; Appold, M.; Didzoleit, H.; Eils, A.; Dietz, C.; Stark, R. W.; Stühn, B.; Gallei, M. Structure Formation of Metallopolymer-Grafted Block Copolymers. *Macromolecules* **2016**, *49* (9), 3415–3426.
- (10) Jackson, A. C.; Beyer, F. L.; Price, S. C.; Rinderspacher, B. C.; Lambeth, R. H. Role of Metal-Ligand Bond Strength and Phase Separation on the Mechanical Properties of Metallopolymer Films. *Macromolecules* **2013**, *46* (14), 5416–5422.
- (11) Jackson, A. C.; Walck, S. D.; Strawhecker, K. E.; Butler, B. G.; Lambeth, R. H.; Beyer, F. L. Metallopolymers Containing Excess Metal-Ligand Complex for Improved Mechanical Properties. *Macromolecules* **2014**, *47* (13), 4144–4150.
- (12) Mavila, S.; Diesendruck, C. E.; Linde, S.; Amir, L.; Shikler, R.; Lemcoff, N. G. Polycyclooctadiene Complexes of Rhodium(I): Direct Access to Organometallic Nanoparticles. *Angew. Chem., Int. Ed.* **2013**, *52* (22), 5767–5770.
- (13) Levy, A.; Feinstein, R.; Diesendruck, C. E. Mechanical Unfolding and Thermal Refolding of Single-Chain Nanoparticles Using Ligand–Metal Bonds. J. Am. Chem. Soc. 2019, 141 (18), 7256–7260.
- (14) Yount, W. C.; Loveless, D. M.; Craig, S. L. Small-Molecule Dynamics and Mechanisms Underlying the Macroscopic Mechanical Properties of Coordinatively Cross-Linked Polymer Networks. *J. Am. Chem. Soc.* **2005**, *127* (41), 14488–14496.
- (15) Rao, Y.-L.; Chortos, A.; Pfattner, R.; Lissel, F.; Chiu, Y.-C.; Feig, V.; Xu, J.; Kurosawa, T.; Gu, X.; Wang, C.; He, M.; Chung, J. W.; Bao, Z. Stretchable Self-Healing Polymeric Dielectrics Cross-Linked Through Metal-Ligand Coordination. *J. Am. Chem. Soc.* **2016**, *138* (18), 6020–6027.
- (16) Li, C.-H.; Wang, C.; Keplinger, C.; Zuo, J.-L.; Jin, L.; Sun, Y.; Zheng, P.; Cao, Y.; Lissel, F.; Linder, C.; You, X-Z.; Bao, Z. A Highly Stretchable Autonomous Self-Healing Elastomer. *Nat. Chem.* **2016**, *8* (6), 618–624.
- (17) Li, C.-H.; Zuo, J.-L. Self-Healing Polymers Based on Coordination Bonds. Adv. Mater. 2019, 1903762.
- (18) Holten-Andersen, N.; Harrington, M. J.; Birkedal, H.; Lee, B. P.; Messersmith, P. B.; Lee, K. Y. C.; Waite, J. H. PH-Induced Metal-Ligand Cross-Links Inspired by Mussel Yield Self-Healing Polymer Networks with near-Covalent Elastic Moduli. *Proc. Natl. Acad. Sci. U. S. A.* **2011**, *108* (7), 2651–2655.
- (19) Grindy, S. C.; Holten-Andersen, N. Bio-Inspired Metal-Coordinate Hydrogels with Programmable Viscoelastic Material Functions Controlled by Longwave UV Light. *Soft Matter.* **2017**, *13* (22), 4057–4065.
- (20) Auletta, J. T.; LeDonne, G. J.; Gronborg, K. C.; Ladd, C. D.; Liu, H.; Clark, W. W.; Meyer, T. Y. Stimuli-Responsive Iron-Cross-Linked Hydrogels That Undergo Redox-Driven Switching between Hard and Soft States. *Macromolecules* **2015**, *48* (6), 1736–1747.
- (21) Balkenende, D. W. R.; Coulibaly, S.; Balog, S.; Simon, Y. C.; Fiore, G. L.; Weder, C. Mechanochemistry with Metallosupramolecular Polymers. *J. Am. Chem. Soc.* **2014**, *136* (29), 10493–10498.
- (22) Di Giannantonio, M.; Ayer, M. A.; Verde-Sesto, E.; Lattuada, M.; Weder, C.; Fromm, K. M. Triggered Metal Ion Release and Oxidation: Ferrocene as a Mechanophore in Polymers. *Angew. Chem. Int. Ed.* **2018**, *57* (35), 11445–11450.
  - (23) Piermattei, A.; Karthikeyan, S.; Sijbesma, R. P. Activating Catalysts with Mechanical Force. Nat. Chem. 2009, 1 (2), 133-137.
- (24) Paulusse, J. M. J.; Sijbesma, R. P. Selectivity of Mechanochemical Chain Scission in Mixed Palladium(Ii) and Platinum(Ii) Coordination Polymers. *Chem. Commun.* **2008**, No. 37, 4416–4418.
- (25) Karthikeyan, S.; Potisek, S. L.; Piermattei, A.; Sijbesma, R. P. Highly Efficient Mechanochemical Scission of Silver-Carbene Coordination Polymers. J. Am. Chem. Soc. 2008, 130 (45), 14968–14969.

- (26) Chen, P.; Li, Q.; Grindy, S.; Holten-Andersen, N. White-Light-Emitting Lanthanide Metallogels with Tunable Luminescence and Reversible Stimuli-Responsive Properties. *J. Am. Chem. Soc.* **2015**, *137* (36), 11590–11593.
- (27) Filonenko, G. A.; Khusnutdinova, J. R. Dynamic Phosphorescent Probe for Facile and Reversible Stress Sensing. *Adv. Mater.* **2017**, 29 (22), 1700563.
- (28) Filonenko, G. A.; Sun, D.; Weber, M.; Müller, C.; Pidko, E. A. Multicolor Organometallic Mechanophores for Polymer Imaging Driven by Exciplex Level Interactions. *J. Am. Chem. Soc.* **2019**, 141 (24), 9687–9692.
- (29) Beyer, M. K. The Mechanical Strength of a Covalent Bond Calculated by Density Functional Theory. J. Chem. Phys. 2000, 112 (17), 7307-7312.
- (30) Ong, M. T.; Leiding, J.; Tao, H.; Virshup, A. M.; Martínez, T. J. First Principles Dynamics and Minimum Energy Pathways for Mechanochemical Ring Opening of Cyclobutene. *J. Am. Chem. Soc.* **2009**, *131* (18), 6377–6379.
- (31) Ribas-Arino, J.; Shiga, M.; Marx, D. Understanding Covalent Mechanochemistry. Angew. Chemie Int. Ed. 2009, 48 (23), 4190-4193.
- (32) Wolinski, K.; Baker, J. Theoretical Predictions of Enforced Structural Changes in Molecules. Mol. Phys. 2009, 107 (22), 2403-2417.
- (33) Stauch, T.; Dreuw, A. Quantum Chemical Strain Analysis For Mechanochemical Processes. Acc. Chem. Res. 2017, 50 (4), 1041–1048.
- (34) Chen, Z.; Mercer, J. A. M.; Zhu, X.; Romaniuk, J. A. H.; Pfattner, R.; Cegelski, L.; Martinez, T. J.; Burns, N. Z.; Xia, Y. Mechanochemical Unzipping of Insulating Polyladderene to Semiconducting Polyacetylene. *Science* **2017**, *357* (6350), 475–479.
- (35) Davis, D. A.; Hamilton, A.; Yang, J.; Cremar, L. D.; Van Gough, D.; Potisek, S. L.; Ong, M. T.; Braun, P. V; Martinez, T. J.; White, S. R.; et al. Force-Induced Activation of Covalent Bonds in Mechanoresponsive Polymeric Materials. *Nature* **2009**, *459* (7243), 68–72.
- (36) Bettens, T.; Alonso, M.; Geerlings, P.; De Proft, F. Implementing the Mechanical Force into the Conceptual DFT Framework: Understanding and Predicting Molecular Mechanochemical Properties. *Phys. Chem. Chem. Phys.* **2019**, *21* (14), 7378–7388.
- (37) Müller, J.; Hartke, B. ReaxFF Reactive Force Field for Disulfide Mechanochemistry, Fitted to Multireference Ab Initio Data. *J. Chem. Theory Comput.* **2016**, *12*, 3913–3925.
- (38) Stauch, T.; Dreuw, A. Force-Induced Retro-Click Reaction of Triazoles Competes with Adjacent Single-Bond Rupture. *Chem. Sci.* **2017**, *8* (8), 5567–5575.
- (39) Krupička, M.; Dopieralski, P.; Marx, D. Unclicking the Click: Metal-Assisted Mechanochemical Cycloreversion of Triazoles Is Possible. *Angew. Chem. Int. Ed.* **2017**, *56* (27), 7745–7749.
- (40) Stauch, T.; Dreuw, A. Predicting the Efficiency of Photoswitches Using Force Analysis. J. Phys. Chem. Lett. 2016, 7 (7), 1298–1302.
- (41) Eloi, J.-C.; Chabanne, L.; Whittell, G. R.; Manners, I. Metallopolymers with Emerging Applications. Mater. Today 2008, 11 (4), 28-36.
- (42) Edwards, D. A.; Hayward, R. N. Transition Metal Acetates. Can. J. Chem. 1968, 46, 3443-3446.
- (43) Ishii, T.; Tsuboi, S.; Sakane, G.; Yamashita, M.; Breedlove, B. K. Universal Spectrochemical Series of Six-Coordinate Octahedral Metal Complexes for Modifying the Ligand Field Splitting. *Dalt. Trans.* **2009**, *4*, 680–687.
- (44) Bauman, J. E.; Wang, J. C. Imidazole Complexes of Nickel(II), Copper(II), Zinc(II), and Silver(I). Inorg. Chem. 1964, 3, 368-373.
- (45) Shao, Y.; Gan, Z.; Epifanovsky, E.; Gilbert, A. T. B.; Wormit, M.; Kussmann, J.; Lange, A. W.; Behn, A.; Deng, J.; Feng, X.; Ghosh, D.; Goldey, M.; Horn, P. R.; Jacobson, L. D.; Kaliman, I.; Khaliullin, R. Z.; Kus, T.; Landau, A.; Liu, J.; et al. Advances in Molecular Quantum Chemistry Contained in the Q-Chem 4 Program Package. *Mol. Phys.* **2015**, *113* (2), 184–215.
- (46) Mardirossian, N.; Head-Gordon, M. ωB97X-V: A 10-Parameter, Range-Separated Hybrid, Generalized Gradient Approximation Density Functional with Nonlocal Correlation, Designed by a Survival-of-the-Fittest Strategy. *Phys. Chem. Chem. Phys.* **2014**, *16*, 9904–9924.

- (47) Weigend, F.; Ahlrichs, R. Balanced Basis Sets of Split Valence, Triple Zeta Valence and Quadruple Zeta Valence Quality for H to Rn: Design and Assessment of Accuracy. *Phys. Chem. Chem. Phys.* **2005**, *7*, 3297–3305.
- (48) Wu, C.; Alqahtani, A.; Sangtarash, S.; Vezzoli, A.; Sadeghi, H.; Robertson, C. M.; Cai, C.; Lambert, C.; Higgins, S.; Nichols, R. In-Situ Formation of H-Bonding Imidazole Chains in Break-Junction Experiments. *ChemRxiv. Preprint.* **2019**.

